Biosensors and Bioelectronics 180 (2021) 113106

Contents lists available at ScienceDirect

Biosensors and Bioelectronics

journal homepage: http://www.elsevier.com/locate/bios

# Simultaneous fluorescence determination of bisphenol A and its halogenated analogs based on a molecularly imprinted paper-based analytical device and a segment detection strategy

Lingshuai Zeng, Xiu Zhang, Xiu Wang, Danqi Cheng, Ruifang Li, Bin Han, Minmin Wu, Zhijia Zhuang, Annan Ren, Yikai Zhou, Tao Jing *

*State Key Laboratory of Environment Health (Incubation), Key Laboratory of Environment and Health, Ministry of Education, Key Laboratory of Environment and Health (Wuhan), Ministry of Environmental Protection, School of Public Health, Tongji Medical College, Huazhong University of Science and Technology, #13 Hangkong Road, Wuhan, Hubei, 430030, China*

ARTICLE INFO

*Keywords:*
Molecularly imprinted polymers
Metal-organic frameworks
Photocatalytic activity
Paper-based analytical device
Fluorescent detection

ABSTRACT

Bisphenol A (BPA) and its halogenated analogs tetrabromobisphenol A (TBBPA) and tetrachlorobisphenol A (TCBPA) are common environmental contaminants and a method for their simultaneous determination is urgently needed. A paper-based analytical device (PAD) was prepared using a metal-organic framework of UiO-66-$NH_2$ coated with molecularly imprinted polymers (MIPs) using TBBPA as a template. The maximum adsorption capacity was 120.94 mg $g^{-1}$ and the imprinting factor was 4.07. The selective recognition ability of this PAD enabled the effective separation of TBBPA, TCBPA and BPA based on paper chromatography. Subsequently, the PAD cut into segments were used individually to determine the presence of target chemicals using a highly sensitive fluorescent method. Under ultraviolet light irradiation, UiO-66-$NH_2$ acts as a photocatalyst to produce reactive oxygen species (ROS) that degrade TBBPA, TCBPA or BPA in the imprinted cavities and the fluorescent signal of 2′,7′-dichlorodihydrofluorescein diacetate ($H_2$DCFDA) added as a ROS probe enabled the indirect determination of target chemicals. This method could determine BPA and its halogenated analogs in dust samples simultaneously with detection limits ranging from 0.14 to 0.30 ng $g^{-1}$. The intraday relative standard deviation (RSD) was ≤6.8% and interday RSD was ≤8.1%. The recoveries ranged from 91.0 to 105.6% with RSD values that were ≤7.5%. The results stemmed from this method were consistent with those obtained from LC-MS/MS. It is an environmentally-friendly approach due to the degradation of target pollutants and possesses many advantages such as high selectivity, low cost and easy-to-fabrication.

## 1. Introduction

Bisphenol A (BPA) is widely used in the manufacture of epoxy resins and polycarbonate plastics as surface coatings for cans, food containers, dental composites and thermal paper (Qiao et al., 2020; Zhang et al., 2019a). Its halogenated analogs tetrabromobisphenol A (TBBPA) and tetrachlorobisphenol A (TCBPA) are often used as reactive or additive flame retardants in various synthetic textiles, electronic equipment, plastic products, furniture and building materials (Gu et al., 2018; Zhang et al., 2019b). Because of the massive production and large consumption of these consumer products, BPA and its halogenated analogs are ubiquitous and coexisting in the environment where BPA, TBBPA and TCBPA are known to occur at 4.69–1000, 10.1–87 and 0.76–0.81 ng $g^{-1}$ with detection rates at 76.9–100, 80.0–96.2 and 15.2–57.7%, respectively (Song et al., 2014b; Wang et al., 2015; Zhu et al., 2019b). These compounds also have been found in human serum and urine (Jin et al., 2018; Li et al., 2020; Ye et al., 2015). BPA, TBBPA and TCBPA are persistent organic pollutants and present endocrine-disrupting effects, cytotoxicity, genotoxicity, immunotoxicity, as well as reproductive toxicity and neurotoxicity (Chen et al., 2016; Lai et al., 2015; Noyes et al., 2019). Thus, an on-site method for their simultaneous determination is of crucial significance for environmental monitoring and human co-exposure assessments.

Conventional analytical methods for simultaneous determination of

* Corresponding author. School of Public Health, Tongji Medical College, Huazhong University of Science and Technology, #13 Hangkong Road, Wuhan, Hubei, 430030, China.
*E-mail address:* jingtao@hust.edu.cn (T. Jing).

https://doi.org/10.1016/j.bios.2021.113106
Received 6 November 2020; Received in revised form 25 January 2021; Accepted 16 February 2021
Available online 20 February 2021

these chemicals primarily rely on mass spectrometric methods (Cheng et al., 2017; Yang et al., 2014) but these methods possess some limitations such as complex instrumentation, high cost, time-consuming pretreatment steps (Letcher and Chu 2010; Liu et al., 2015). Rapid methods also have been developed for BPA determination including electrochemistry, fluorometry and colorimetry (Abnous et al., 2018; Alkasir et al., 2015; Lu and Xu 2017; Shi et al., 2018). However, these methods can only be applied for BPA and not be used in the synchronous analysis for multiple compounds. Paper chromatography can be used as a tool to separate multiple analytes (Weatherston et al., 2018; Zhang et al., 2017), and paper-based analytical devices (PADs) using different types of detectors are more economical, simple, portable and disposable (Akyazi et al., 2018; Mettakoonpitak et al., 2020; Noviana et al., 2020). Thus, PADs integrated with separation and detection that can be used for the simultaneous determination of multiple compounds have been reported previously (Weatherston et al., 2018; Zhao et al., 2017). However, the main drawback is the low theoretical plate number because of the low adsorption capacity and poor selectivity of paper as a substrate. Up to now, paper materials are primarily used to construct the microfluidic channels of PADs (Noviana et al., 2019; Pungjunun et al., 2019). Molecularly imprinted polymers (MIPs) also known as plastic antibodies are useful sorbents for specific recognition for template molecules (Díaz-Liñán et al., 2021; Liu et al., 2016; Mendes et al., 2017; Turiel and Martín-Esteban 2019). Metal-organic frameworks (MOFs) have uniform and tunable pore sizes, large specific surface areas, structural diversity and robust stability (Gutierrez-Serpa et al., 2019; Ramanayaka et al., 2019). Compared with the common MIPs, MOF-based MIPs can achieve a higher specific surface area and a faster mass-transfer rate (Guo et al., 2016; Iskierko et al., 2016; Liu et al., 2017a). Thus, these composites can be formed on the filter paper to improve theoretical plate numbers and further achieve a highly efficient chromatography separation.

Another important factor for BPA and its halogenated analogs detection is the compatibility between chromatographic separation and a highly sensitive detection method. For BPA and its halogenated

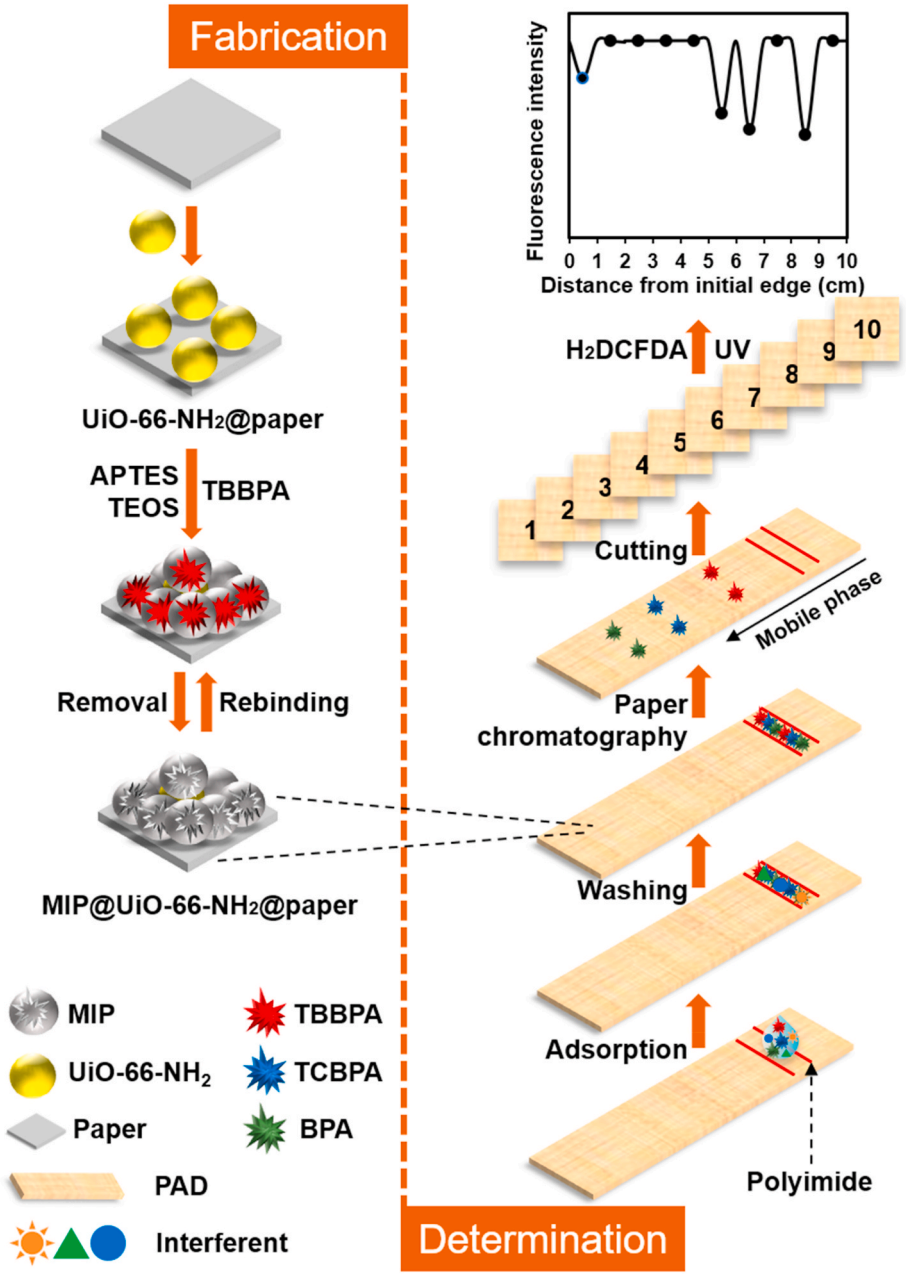


**Fig. 1.** Schematic illustration for the preparation of MIP@UiO-66-$NH_2$@paper and associated analysis procedures.

analogs, there is no known chemical reaction to produce significant color output. Electrochemical detection (Abnous et al., 2018; Ekomo et al., 2018; Yakubu et al., 2020) can substitute but suffers from lower sensitivity due to the short contact time under the flow conditions. Fluorescence detection is a simple, rapid and sensitive approach and is suitable for on-site detection. The UiO-66-$NH_2$ used for the MOF-based MIPs has excellent photocatalytic activity. UiO-66-$NH_2$ can be used for the photocatalytic degradation of organic pollutants utilizing reactive oxygen species (ROS), such as norfloxacin, rhodamine, tetracycline, methylene blue and cationic dyes (Li et al., 2016a; Liang et al. 2017, 2018; Ríos-Gómez et al., 2018; Yang et al., 2019). We found that BPA and its halogenated analogs can also be degraded by UiO-66-$NH_2$ to consume ROS. Thus, 2′,7′-dichlorodihydrofluorescein diacetate ($H_2$DCFDA) as a ROS probe can be used for quantitative analysis of target chemicals. This method adds an environmentally-friendly feature due to the degradation of target pollutants. However, the photocatalytic degradation needs enough time and specific solvents that can affect chromatographic separation and these two procedures are not suitable for a synchronous operation. Thus, following chromatographic separation, paper composites can be cut into segments to establish clear distinctions between the sample matrix, BPA and its halogenated analogs. The target chemical in each segment can be determined by the fluorescent methods using different operation procedures and solvents. This type of chromatographic separation and segmental detection has the potential to promote the development of microfluidic PADs.

In this work, MOF-based MIPs were prepared on filter paper using TBBPA as a template. A microfluidic PAD integrated with MIPs-based paper chromatographic separation and detection was developed for the simultaneous determination of BPA and its halogenated analogs. The mechanisms of selective recognition and photocatalytic degradation were studied in detail. And then it was applied to determine target chemicals in real dust samples. The proposed method displays the potential application to the on-site determination of multicomponent mixtures in complex samples.

## 2. Experimental

### 2.1. Reagents and materials

TBBPA, TCBPA, TBBPA bis(2,3-dibromopropyl ether) (TBBPA-BDBPE), TBBPA bis(allyl ether) (TBBPA-BAE) and TBBPA bis(2-hydroxyethyl ether) (TBBPA-BHEE), BPA, bisphenol F (BPF), bisphenol S (BPS), zirconium chloride ($ZrCl_4$), 2-aminoterephthalic acid, isopropyl alcohol (IPA), benzoquinone (BQ), ethylenediaminetetraacetic acid disodium salt (EDTA-2Na) were purchased from Aladdin Chemical Reagent (Shanghai, China). (3-aminopropyl) triethoxysilane (APTES), tetraethyl orthosilicate (TEOS) and $H_2$DCFDA were purchased from Sigma Chemical (St. Louis, MO, USA). Acetic acid, ethanol, methanol, N, N-dimethylformamide (DMF), hydrochloric acid (HCl), sodium carbonate ($Na_2CO_3$), sodium hydrogencarbonate ($NaHCO_3$) were purchased from Sinopharm Chemical Reagent (Shanghai, China). Ultrapure water was obtained from a Milli-R04 purification system (Millipore, Darmstadt, Germany). Polyimide solution (20 wt%) was purchased from Changzhou Friend Plastic New Material Co., Ltd. (Changzhou, China). HPLC-grade n-hexane, acetone and methanol were obtained from Fisher Chemical (Fair Lawn, NJ, USA). Whatman chromatography paper (200 × 200 mm) was obtained from GE Healthcare Worldwide (Shanghai, China).

### 2.2. Instruments and measurements

The scanning electron microscope (SEM) images were carried out on a Zeiss Gemini 300 SEM (Oberkochen, Germany). The particle size distribution was performed on a Beckman Coulter Delsa Nano C particle analyzer (Osaka, Japan). Surface areas and pore size distributions were measured with a Micromeritics ASAP 2020 volumetric adsorption analyzer (Norcross, GA, USA). Fourier transform infrared spectra (FT-IR) were tested on a Bruker Vertex 70 FTIR Spectrometer (Ettinger, Germany). Thermogravimetric analysis (TGA) was recorded by a PerkinElmer Diamond TG/DTA instrument (Massachusetts, USA). The fluorescence emission spectra were performed on a Lengguang F97Pro fluorophotometer (Shanghai, China). Dust sample verification tests were performed using an Agilent 1200 liquid chromatography-tandem mass spectrometry (LC-MS/MS) system (MA, USA).

### 2.3. Preparation of MIP@UiO-66-$NH_2$@ paper

The UiO-66-$NH_2$ was prepared as the previously reported method (Li et al., 2018b) and the synthetic process was described in detail in the supplementary material. Then, UiO-66-$NH_2$ (100 mg) was dispersed in 20 mL ethanol by ultrasonication for 30 min to form a homogeneous solution. The filter paper was activated in a 5 M $H_2O_2$ solution to obtain enough hydroxyl groups. UiO-66-$NH_2$ was immobilized on filter paper (10 × 10 cm) by suction filtration under negative pressure to fabricate the UiO-66-$NH_2$@paper. For MIP polymerization, 136 mg of TBBPA, 0.234 mL of APTES, 0.278 mL of TEOS and 2 mL of 0.1 M acetic acid were added to 40 mL ethanol under bath sonication to form a homogeneous pre-polymerized solution. The UiO-66-$NH_2$@paper was immersed in this solution and allowed to stand at 60 °C for 24 h. The resulting polymers were thoroughly washed using methanol/acetic acid (v/v, 9/1) to remove unreacted components and templates and vacuum dried at 45 °C. The non-imprinted composites (NIP@UiO-66-$NH_2$@-paper) as control were prepared under the same conditions but lacked template molecules (Fig. 1).

### 2.4. Simultaneous determination of BPA and its halogenated analogs in dust samples

Indoor dust samples were collected from laboratories and student offices in Wuhan, China. The dust samples were obtained from the surface of furniture, floor and windowsills in each room and swept onto aluminum foil using wool paintbrushes. All collected samples were sieved through 212 μm sieves to represent the indoor settled dust, packed in clean aluminum foil and stored at −20 °C until analysis. To prevent cross-contamination, the wool paintbrushes and sieves were washed with methanol and ultrapure water between sampling intervals and then air-dried (Liu et al., 2017b).

TBBPA, TCBPA and BPA in dust samples were extracted with 3 mL n-hexane/acetone solution (3/1, v/v) per 100 mg sample and then sonicated for 10 min, vortexed for 2 min and centrifuged at 5000 rpm for 10 min. The supernatants were collected into glass tubes and the extraction steps were repeated three times. Supernatants were combined and evaporated to dryness under a nitrogen flow and the residue was dissolved in 0.1 mL acetonitrile.

The MIP@UiO-66-$NH_2$@paper was cut into strips (10 × 0.5 cm) to develop a PAD and a sample extraction zone was fabricated by the printing application of polyimide (20 wt%) served as a hydrophobic channel. A stainless steel slice (thickness 0.5 mm) was used for painting polyimide channels on both sides of the PAD as Fig. 1. The extraction solution (2 μL × 5 times) was placed onto the extraction zone and heated at 50 °C for 1 min to adsorb the target chemicals. Because of the presence of hydrophobic zones, water (25 μL × 2 times) was introduced to remove the sample matrix and then removed by using negative pressure. Afterward, methanol/acetic acid (v/v, 9/1) as a mobile phase was used for the separation of TBBPA, TCBPA and BPA on PAD. When the mobile phase migrated to the end of the PAD, the PAD was dried at 50 °C and then cut into 10 equal segments. Afterward, 25 μL $H_2$DCFDA and 475 μL 0.1 M $Na_2CO_3$–$NaHCO_3$ were added to each segment and the mixture was incubated under ultraviolet light (UV) irradiation (365 nm) for 10 min. The UV was produced by a portable UV lamp (365 nm, 10 Watt, HITACHI) that was suitable for on-site detection. The fluorescence intensity was recorded on a microplate reader (BioTek Synergy 2,

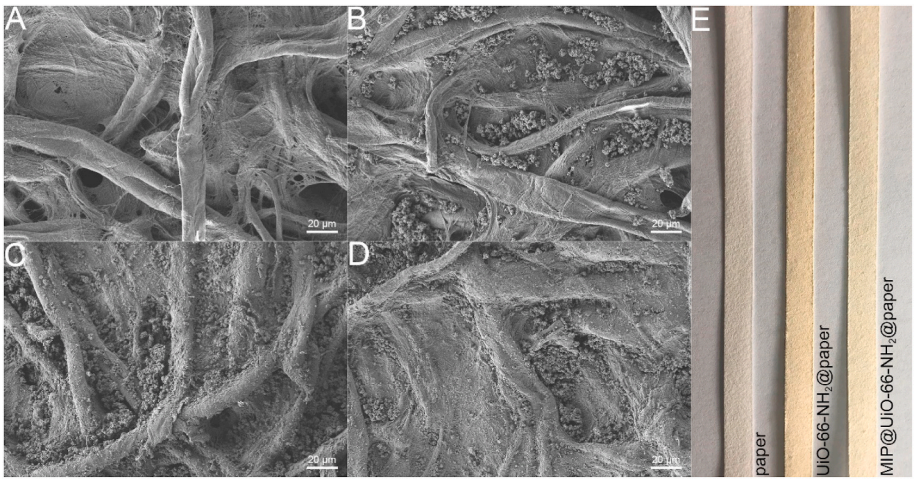


**Fig. 2.** SEM images of (A) paper, (B) UiO-66-$NH_2$@paper, (C) MIP@UiO-66-$NH_2$@paper and (D) NIP@UiO-66-$NH_2$@paper. (E) Photographs of paper, UiO-66-$NH_2$@paper and MIP@UiO-66-$NH_2$@paper.

Winooski, VT, USA) with an excitation maximum at 485/20 nm and an emission maximum at 528/20 nm (Fig. 1).

## 3. Results and discussion

### 3.1. Characterization of MIP@UiO-66-$NH_2$@paper

UiO-66-$NH_2$ was chosen to prepare MIP composites because of its high structural stability in water and photocatalytic activity. As displayed in the SEM picture, the synthesized UiO-66-$NH_2$ particles were uniform with average sizes of 200–300 nm. The particle size of UiO-66-$NH_2$ was 242.1 ± 32.2 nm, which was consistent with the result of SEM. Surface areas and average pore diameters of the particles were 944.20 $m^2$ $g^{-1}$ and 1.42 nm, respectively (Figure S1). UiO-66-$NH_2$ particles were then immobilized in the paper cavities via the hydrogen bond interaction. After the preparation of MIP film on the surface of UiO-66-$NH_2$@paper, the cellulose fibers then appeared rough (Fig. 2). This indicated that the MIP@UiO-66-$NH_2$ composites were successfully constructed on the paper surface.

Elemental analysis of the filter paper, as well as UiO-66-$NH_2$@paper and MIP@UiO-66-$NH_2$@paper indicated the presence of Zr that was an indicator of UiO-66-$NH_2$ immobilization. After MIP polymerization, the subsequent appearance of Si confirmed the successful preparation of MIP@UiO-66-$NH_2$@paper (Figure S2A). The FT-IR spectrums indicated that the peaks at 1629 $cm^{-1}$ (N–H), 1340 $cm^{-1}$ and 1257 $cm^{-1}$ (C–N) could be attributed to the amino group of 2-aminoterephthalic acid in UiO-66-$NH_2$ (Chakarova et al., 2019; Sarker et al., 2018). The band at 1560 $cm^{-1}$ was derived from the amine group of APTES (Senthilkumaran et al., 2020). The adsorption peak at 1055 $cm^{-1}$ corresponded to the stretching vibration of Si–O–Si and the band at 764 $cm^{-1}$ corresponded to the stretching vibration of the Si–O bond (Figure S2B) (Azat et al., 2019; Hu et al., 2021). These results indicated the formation of a MIP film that could selectively recognize BPA and its halogenated analogs.

The TGA curves for the filter paper, UiO-66-$NH_2$@paper and MIP@UiO-66-$NH_2$@paper indicated water evaporation at temperatures <100 °C. At 300–370 °C, the sharp weight losses of the paper (81.36%), UiO-66-$NH_2$@paper (73.90%) and MIP@UiO-66-$NH_2$@paper (67.44%) were caused by the thermal degradation of the filter paper. Slower rates of mass loss for UiO-66-$NH_2$@paper (6.91%) and MIP@UiO-66-$NH_2$@paper (7.99%) were observed at 360–600 °C due to the immobilization of UiO-66-$NH_2$ and formation of a MIP film (Figure S2C).

### 3.2. Adsorption properties of MIP@UiO-66-$NH_2$@paper

A high adsorption capacity is an important factor for MIP composites. The adsorption capacity of MIP@UiO-66-$NH_2$@paper for TBBPA was 61.96 mg $g^{-1}$ in a 100 μg $mL^{-1}$ TBBPA solution and for NIP@UiO-66-$NH_2$@paper was 22.58 mg $g^{-1}$. The UiO-66-$NH_2$@paper did not adsorb TBBPA (Fig. 3A). Similar to MIP composites, NIP composites were also prepared with functional monomer APTES that played an important role in the recognition of TBBPA. Therefore, NIP composites had adsorption capacity for TBBPA. The difference is that MIP composites were equipped with specific stereoscopic cavities and recognition sites, but the adsorption of NIP composites was non-specific adsorption owing to lacking tailor-made imprinting sites (Li et al., 2018a). As a result, compared with MIP composites, NIP composites had a lower adsorption capacity. These results indicated the successful

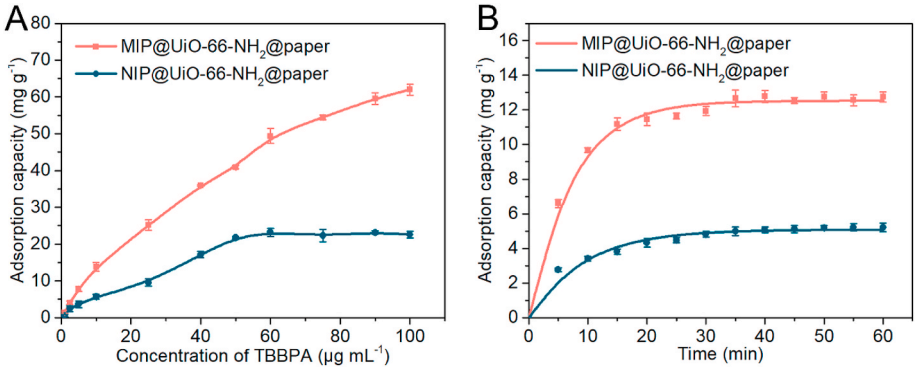


**Fig. 3.** (A) Adsorption isotherms curves with adsorption time of 12 h. (B) Adsorption kinetics curves using an initial concentration of TBBPA of 10 μg $mL^{-1}$.

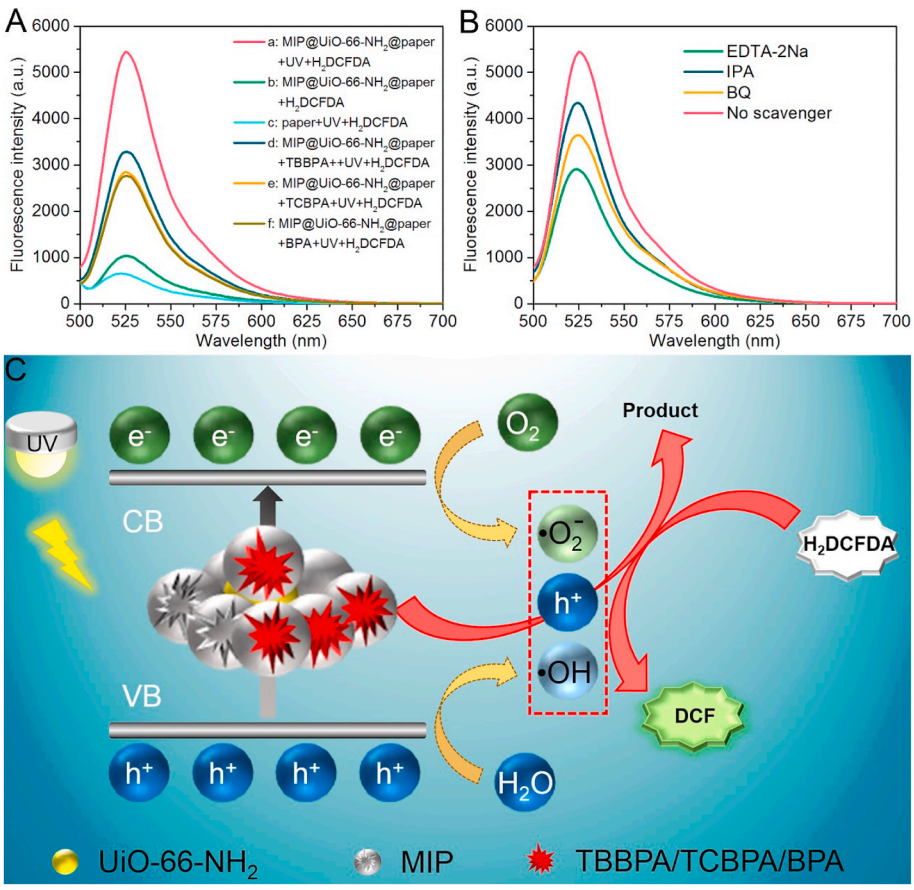


**Fig. 4.** Fluorescence emission spectra of (A) (a) MIP@UiO-66-$NH_2$@paper and $H_2$DCFDA after UV irradiation, (b) MIP@UiO-66-$NH_2$@paper and $H_2$DCFDA without UV irradiation, (c) filter paper and $H_2$DCFDA after UV irradiation, (d) TBBPA, (e) TCBPA and (f) BPA on MIP@UiO-66-$NH_2$@paper and $H_2$DCFDA after UV irradiation. (B) MIP@UiO-66-$NH_2$@paper and $H_2$DCFDA with the addition of different scavengers after UV irradiation. (C) A proposed mechanism for the fluorescent determination of TBBPA, TCBPA and BPA.

construction of highly selective imprinted sites. We further studied the interaction of TBBPA with MIP@UiO-66-$NH_2$@paper using the Langmuir and Freundlich isotherms. The better fit was the Langmuir model that demonstrated that TBBPA binding represented a monolayer surface adsorption. The maximum adsorption capacities ($Q_m$) of MIP and NIP composites were 120.94 and 29.74 mg $g^{-1}$, respectively with an imprinting factor of 4.07 (Table S1).

An analysis of the adsorption kinetics indicated that the adsorption amount of MIP composites could reach 9.92 mg $g^{-1}$ in a 10 μg $mL^{-1}$ TBBPA solution in 10 min. Subsequently, an increase of adsorption time increased the adsorption capacity slowly and equilibrium was reached at 30 min. The result indicated that the removal of the template molecules resulted in residue imprinted channels sufficient for the rapid recognition of TBBPA (Fig. 3B). Compared with other MIPs whose equilibrium times were over 60 min (Shao et al., 2017; Wu et al., 2018), the short equilibrium time in this study can be attributed to recognition cavities formed by the surface imprinting technology as well as extensive surface areas and high porosity provided by the UiO-66-$NH_2$ (Li et al., 2018a). Furthermore, pseudo-first-order kinetic, pseudo-second-order kinetic, and Weber-Morris models were employed to investigate the mechanism involved in the adsorption process. The theoretical adsorption capacities calculated from pseudo-second-order kinetic models were the closest fits to the experimental observations. Therefore, TBBPA adsorption onto MIP@UiO-66-$NH_2$@paper was most likely chemisorption. Moreover, the Weber-Morris model for the MIP composites showed multi-linearity, suggesting a two-step adsorption process attributed to the spread from the aqueous phase to the external surface and the gradual adsorption of TBBPA. Intraparticle diffusion was the rate-limiting step (Table S2).

### 3.3. The mechanism of fluorescent detection

The degradation of TBBPA, TCBPA and BPA also occurs during fluorescent detection and this fluorescent detection is therefore an environmentally friendly method. Compared with pure filter paper, MIP@UiO-66-$NH_2$@paper exhibited strong fluorescence under UV irradiation when it was incubated with $H_2$DCFDA as a ROS probe. However, this mixture had a weak fluorescence signal in the absence of UV irradiation, implying a photocatalytic activity for UiO-66-$NH_2$. After the introduction of TBBPA, TCBPA or BPA, the fluorescence intensity was significantly decreased (Fig. 4A). The levels of target chemicals in incubating solutions containing UiO-66-$NH_2$@paper were determined by the LC-MS/MS method. The target chemicals were greatly decreased following UV irradiation during the incubation period. Moreover, the UiO-66-$NH_2$@paper did not display any obvious adsorption of target chemicals, indicating that the low levels were a result of degradation rather than adsorption (Figure S3). Therefore, UiO-66-$NH_2$ could be used as a photocatalyst for degradation of BPA, TCBPA and TBBPA that would further consume ROS and cause a decrease in fluorescence intensity.

Hydroxyl radical (·OH), superoxide anion radical ($\cdot O_2^-$) and holes ($h^+$) are the primary active species involved in the photocatalytic process (Hu et al., 2016; Tang et al., 2018). Therefore, we performed reactive species trapping experiments to investigate the photocatalytic mechanism of UiO-66-$NH_2$. IPA, BQ and EDTA-2Na were used to identify the presence of ·OH, $\cdot O_2^-$ and $h^+$ during the photocatalytic process, respectively. The fluorescence intensity was significantly decreased with the addition of EDTA-2Na, implying that $h^+$ was the major active species in the photocatalytic process of UiO-66-$NH_2$. The presence of IPA and BQ could partially inhibit the fluorescence intensity, suggesting that ·OH and $\cdot O_2^-$ were secondary active species (Fig. 4B).

These findings allowed the development of a hypothesis that under UV irradiation, UiO-66-$NH_2$ adsorbs photons with energy higher than its bandgap so that the electron-hole pairs are separated. A large number of photoinduced excited electrons ($e^-$) transfer from the valence band (VB)

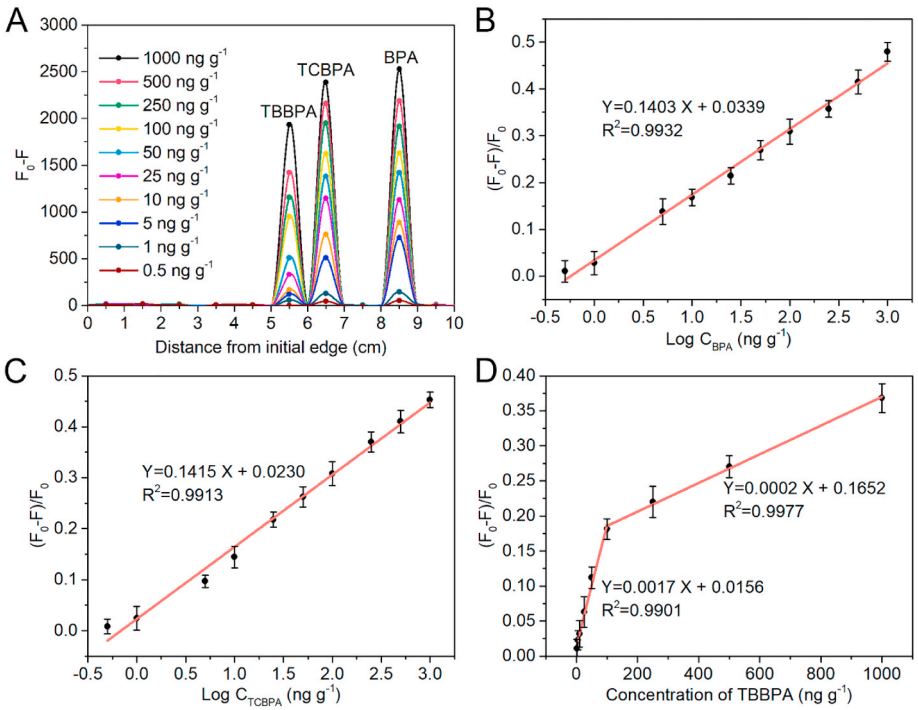


**Fig. 5.** (A) Paper chromatography separation and fluorescent detection of TBBPA, TCBPA, and BPA using a paper-based analytical device. Linear calibration plots for (B) BPA, (C) TCBPA and (D) TBBPA.

to the conduction band (CB). Subsequently, the $e^-$ reacts with dissolved oxygen to form $\cdot O_2^-$. At the same time, the $h^+$ remaining in the VB can oxidize water molecules to generate ·OH (Fig. 4C). These active species that included ·OH, $\cdot O_2^-$ and $h^+$ generated by UiO-66-$NH_2$ were then responsible for the degradation of TBBPA, TCBPA and BPA adsorbed onto the MIP@UiO-66-$NH_2$@paper. Residual radicals can oxidize $H_2$DCFDA as a ROS probe to its fluorescent state 2′,7′-dichlorofluorescein (DCF). At the same time, the photocatalytic properties of MIP@UiO-66-$NH_2$@paper were weakened due to the selective adsorption of the target chemicals. Based on this, we propose a dual amplification strategy for the highly sensitive determination of BPA and its halogenated analogs (Fig. 4C).

### 3.4. Optimization of separation and detection conditions

For effective absorption of BPA and its halogenated analogs from dust extract, methanol, ethanol and acetonitrile were tested as the extraction and then spotting solvents. These solvents did not significantly affect the adsorption effect (Figure S4). However, when acetonitrile was used for the spotting solvent, the dust extract would not go beyond the sample extraction zone by diffusion. After the solvent evaporation, water was used to remove the sample matrix because of hydrophobic target chemicals. The choice of mobile phase was crucial for paper chromatographic separation. Methanol and acetic acid were the regular elution solvents for the elution of target analytes in MIP composites. The solubility of target chemicals in methanol is the greatest, which was beneficial to elution. Methanol with acetic acid was able to break hydrogen bonds between hydroxyl groups of target chemicals and amino groups present in MIP cavities (Chen et al., 2011; Lu et al., 2019). Thus, methanol and acetic acid were chosen as the mobile phase and further optimized. With an increase of acetic acid, the separation efficiency was greatly improved. When the ratio of methanol and acetic acid was 9:1, BPA, TCBPA and TBBPA could be simultaneously determined in real samples. The compounds were eluted in the order of BPA > TCBPA > TBBPA based on the selective recognition of the MIPs for the target chemicals (Figure S5). Furthermore, the flow rate was optimized by controlling the placed angle of MIP@UiO-66-$NH_2$@-paper. We found that there was no significant difference and the change in flow rate accomplished by this procedure did not affect the separation efficiency. Thus, to save time and cost, MIP@UiO-66-$NH_2$@paper was vertically placed for the separation of BPA and its halogenated analogs.

We also optimized the pH, $H_2$DCFDA concentration and irradiation time in this study. The fluorescence quenching efficiency was expressed as $(F_0 - F)/F_0$, where $F_0$ and F are the fluorescence intensity of the mixture in the absence and presence of the target chemicals, respectively. The pH strongly affected the fluorescence intensity of the reaction system and the intensity was maximal at pH 9.0 with a significant decrease at lower and higher pH values. Additionally, fluorescent intensity was increased with the higher levels of $H_2$DCFDA and the optimized fluorescence quenching effect was obtained at 75 μM. An optimization of irradiation time indicated that the degradation of TBBPA, TCBPA and BPA reached equilibrium at 10 min and then ROS consumption was decreased (Figure S6).

### 3.5. Analytical performance of the fluorescent method

In this study, a microfluidic PAD with MIP-based paper chromatographic separation and detection were developed for the simultaneous determination of BPA and its halogenated analogs in environmental samples. The fluorescence intensities were proportional to the concentrations or logarithm concentrations of BPA, TCBPA and TBBPA. The linear ranges were 0.5–1000 ng $g^{-1}$ for BPA and TCBPA and 1–1000 ng $g^{-1}$ for TBBPA. All correlation coefficients were ≥0.99 indicating excellent linearity. The limit of detection (LOD) (defined as 3 σ/s, where σ is the standard deviation for 10 blanks and s is the slope of the calibration curve) was 0.16 ng $g^{-1}$ for BPA, 0.14 ng $g^{-1}$ for TCBPA and 0.30 ng $g^{-1}$ for TBBPA (Fig. 5). Compared with previously reported methods (Correia-Sá et al., 2018; Deiminiat et al., 2017; Dong et al., 2015; Feng et al., 2019; Fu et al., 2020; Gao et al., 2017; Jurek and Leitner 2018; Li et al., 2016b; Liu et al., 2019; Lu and Xu 2017; Song et al., 2019; Wang et al. 2016a, 2016b, 2018; Yakubu et al., 2020), our method possessed a wider linear range and a relatively lower LOD (Table S3). Our novel

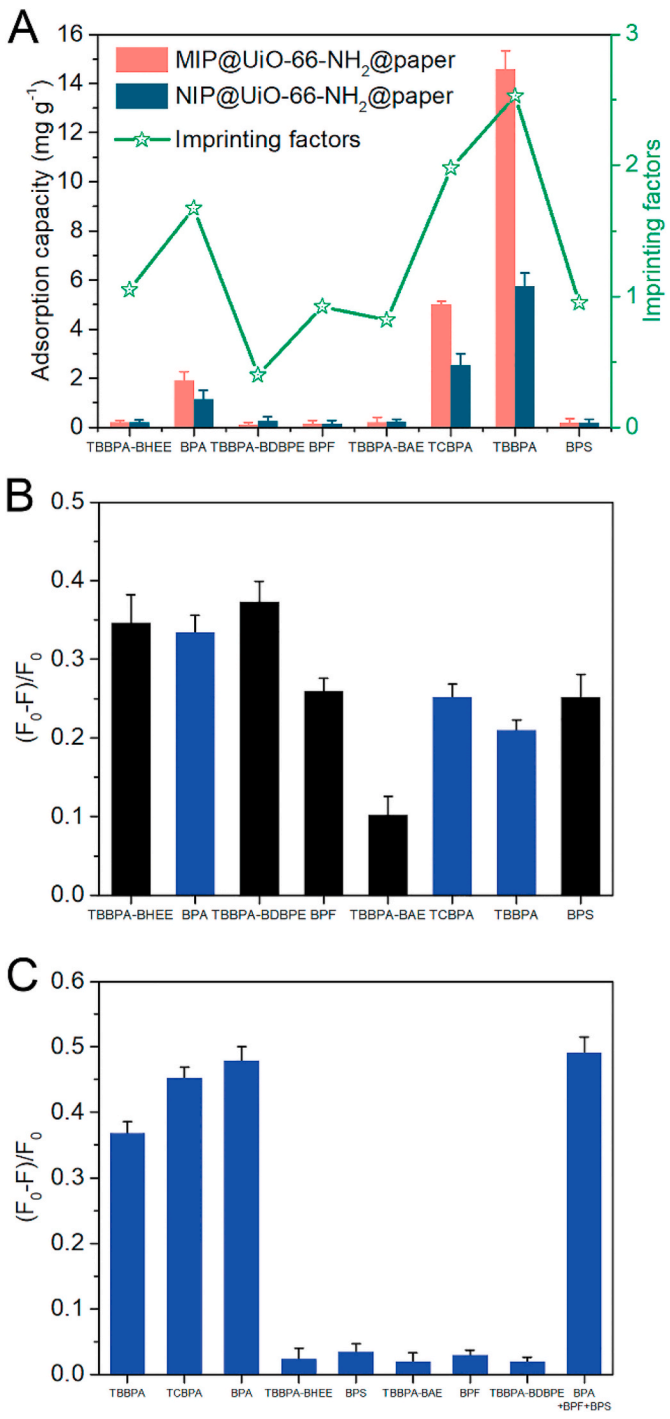


**Fig. 6.** (A) Selective adsorption of MIP@UiO-66-$NH_2$@paper and NIP@UiO-66-$NH_2$@paper for 10 μg $mL^{-1}$ of TBBPA and structural analogs. (B) Photocatalytic selectivity of UiO-66-$NH_2$ for TBBPA, TCBPA, BPA and structural analogs using UiO-66-$NH_2$@paper. (C) The selectivity of the fluorescent method towards TBBPA, TCBPA, BPA and structural analogs using MIP@UiO-66-$NH_2$@paper.

method could simultaneously determine BPA and its halogenated analogs with advantages including low cost, wide availability, simplicity, easy operation, high sensitivity and environmental friendliness.

We further evaluated the selectivity of the proposed method for TBBPA, TCBPA, BPA and their structural analogs including BPF, BPS, TBBPA-BHEE, TBBPA-BDBPE and TBBPA-BAE. The adsorption capacities of MIP@UiO-66-$NH_2$@paper for TBBPA, TCBPA and BPA were higher than all the structural analogs (Fig. 6A). Furthermore, the UiO-66-$NH_2$@paper was confirmed to have photocatalytic activities for all tested chemicals and the degradation efficiencies of these chemicals are different (Fig. 6B). Significant changes in fluorescence intensities were obtained with TBBPA, TCBPA and BPA based on the MIP@UiO-66-$NH_2$@paper and only a slight change was associated with the other structural analogs (Fig. 6C). After chromatographic separation, BPA, BPF and BPS were co-eluted in the same segment of MIP@UiO-66-$NH_2$@paper, but BPF and BPS did not interfere with the determination of BPA. This indicated that the selective adsorption of MIP composites plays an important role in fluorescence detection. There was almost no change in the fluorescence intensity for blank dust samples defined by the LC-MS/MS method. These results implied that the sample matrix did not affect the determination of BPA and its halogenated analogs and background noise was not enhanced under our detection conditions.

The precision of the method was investigated using both intraday and interday replicates. The intraday relative standard deviation (RSD) was ≤6.8% and interday RSD was ≤8.1%. These PADs were also stable in storage with RSD values of 6.0% (TBBPA), 4.8% (TCBPA) and 7.2% (BPA) when the MIP composites were stored at room temperature for 4 weeks (Figure S7). Long-term storage did not significantly affect the performance of PDA. The reproducibility was studied using different MIP composites (n = 5) prepared in the same way and the RSD values were ≤6.2%. These results indicated that these PADs can be of practical use in the field.

### 3.6. Analytical application in real dust samples

Under the optimized conditions, we applied the proposed method for the simultaneous determination of TBBPA, TCBPA and BPA in real dust samples and the results were compared to the classical LC-MS/MS method. Spiked recoveries ranged from 91.0 to 105.6% with RSD values that were ≤7.5%. These found values were in good agreement with those obtained by the LC-MS/MS method ($R^2 = 0.9975$) (Table S4). These results indicated that the proposed method can be used to simultaneously determine BPA and its halogenated analogs in real dust samples with excellent applicability and feasibility. It has been reported that BPA was detected in a concentration range of nd-37000 (mean: 234) ng $g^{-1}$ with the detection frequency of 98.3% in the dust (Zhu et al., 2020), and found in 100% of dust samples ranging from 9.6 to 32,000 (mean: 1000) ng $g^{-1}$ (Wang et al., 2015). TBBPA was found in road dust ranging from <0.06 to 74.1 (mean: 20.7) ng $g^{-1}$ in Chongqing, China (Lu et al., 2018), and detected in 80% of dust samples at a concentration that ranged from <1 to 2300 (mean: 87) ng $g^{-1}$ in twelve countries (Wang et al., 2015). Researches on the occurrence of TCBPA in the dust is skimpy. It has been reported that TCBPA was found in 14.9% of dust samples ranging from 0 to 6.88 ng $g^{-1}$ in China (Jia et al., 2019). TCBPA was also found in 57.7% of sludge samples ranging from 0.29 to 143 ng $g^{-1}$, and detected in 15.2% of sludge samples in a range of 0.0735–11.5 ng $g^{-1}$ in China (Song et al., 2014a; Zhu et al., 2019a). In our study, BPA and TBBPA were found in all dust samples in a range of 56.8–210.7 and 176.5–846.8 ng $g^{-1}$, respectively, which equaled to these reported studies. Although TCBPA was not detected, BPA, TBBPA and TCBPA have been reported to be co-existing in indoor dust and sewage sludges (Jia et al., 2019; Song et al., 2014b; Wang et al., 2015; Zhu et al., 2019b). Therefore, the proposed method is necessary for the simultaneous determination of BPA, TBBPA and TCBPA in environmental samples.

## 4. Conclusions

In this study, a proposed method was developed for the simultaneous determination of TBBPA, TCBPA and BPA in real dust samples, based on the molecularly imprinting recognition and a segment fluorescence detection strategy. Paper chromatographic separation and sensitive detection were integrated into the PAD by using MIP@UiO-66-$NH_2$@paper. The presence of UiO-66-$NH_2$ enhanced the selective recognition performance of the MIP films and the internal photocatalytic

activity was able to degrade target chemicals enabling highly sensitive fluorescent detection. Furthermore, a signal amplification strategy was also developed for the simultaneous determination of BPA and its halogenated analogs in real samples with detection limits that ranged from 0.14 to 0.30 ng $g^{-1}$. The proposed method holds significant promise to simultaneously determine multiple pollutants in real samples and its advantages are high sensitivity, low cost, easy-to-fabrication and environmental friendliness. This method is suitable for on-site detection for environmental monitoring and human co-exposure assessments.

## CRediT authorship contribution statement

**Lingshuai Zeng:** Methodology, Formal analysis, Data curation, Software, Writing – original draft. **Xiu Zhang:** Investigation, Characterization, Visualization. **Xiu Wang:** Validation, Software. **Danqi Cheng:** Formal analysis, Software. **Ruifang Li:** Visualization, Software. **Bin Han:** Formal analysis, Writing – review & editing. **Minmin Wu:** Formal analysis, Writing – review & editing. **Zhijia Zhuang:** Formal analysis, Writing – review & editing. **Annan Ren:** Formal analysis, Writing – review & editing. **Yikai Zhou:** Conceptualization, Funding acquisition, Writing – review & editing. **Tao Jing:** Supervision, Funding acquisition, Conceptualization, Project administration, Journal Preproof, Writing – review & editing.

## Declaration of competing interest

The authors declare that they have no known competing financial interests or personal relationships that could have appeared to influence the work reported in this paper.

## Acknowledgments

This research was funded by the National Natural Science Foundation of China (No. 22076054 and 21577042). The Center of Analysis and Testing of Huazhong University of Science and Technology was acknowledged for their help with the SEM, FT-IR, EDX and TGA analysis.

## Appendix A. Supplementary data

Supplementary data to this article can be found online at https://doi.org/10.1016/j.bios.2021.113106.

## References

Abnous, K., Danesh, N.M., Ramezani, M., Alibolandi, M., Taghdisi, S.M., 2018. Biosens. Bioelectron. 119, 204–208.
Akyazi, T., Basabe-Desmonts, L., Benito-Lopez, F., 2018. Anal. Chim. Acta 1001, 1–17.
Alkasir, R.S.J., Rossner, A., Andreescu, S., 2015. Environ. Sci. Technol. 49 (16), 9889–9897.
Azat, S., Korobeinyk, A.V., Moustakas, K., Inglezakis, V.J., 2019. J. Clean. Prod. 217, 352–359.
Chakarova, K., Strauss, I., Mihaylov, M., Drenchev, N., Hadjiivanov, K., 2019. Microporous Mesoporous Mater. 281, 110–122.
Chen, D., Kannan, K., Tan, H., Zheng, Z., Feng, Y.-L., Wu, Y., Widelka, M., 2016. Environ. Sci. Technol. 50 (11), 5438–5453.
Chen, F.-F., Wang, G.-Y., Shi, Y.-P., 2011. J. Separ. Sci. 34 (19), 2602–2610.
Cheng, Y., Nie, X.-m., Wu, H.-q., Hong, Y.-h., Yang, B.-c., Liu, T., Zhao, D., Wang, J.-f., Yao, G.-h., Zhang, F., 2017. Anal. Chim. Acta 950, 98–107.
Correia-Sá, L., Norberto, S., Delerue-Matos, C., Calhau, C., Domingues, V.F., 2018. J. Chromatogr. B 1072, 9–16.
Deiminiat, B., Rounaghi, G.H., Arbab-Zavar, M.H., Razavipanah, I., 2017. Sens. Autuators B Chem. 242, 158–166.
Díaz-Liñán, M.C., García-Valverde, M.T., Lucena, R., Cárdenas, S., López-Lorente, A.I., 2021. Microchem. J. 160, 105686.
Dong, L.-J., Tan, Z.-Q., Chen, M., Liu, J.-F., 2015. Anal. Methods 7 (4), 1380–1386.
Ekomo, V.M., Branger, C., Bikanga, R., Florea, A.-M., Istamboulie, G., Calas-Blanchard, C., Noguer, T., Sarbu, A., Brisset, H., 2018. Biosens. Bioelectron. 112, 156–161.
Feng, J., Tao, Y., Shen, X., Jin, H., Zhou, T., Zhou, Y., Hu, L., Luo, D., Mei, S., Lee, Y.-I., 2019. Microchem. J. 144, 93–101.
Fu, H.-J., Wang, Y., Xiao, Z.-L., Wang, H., Li, Z.-F., Shen, Y.-D., Lei, H.-T., Sun, Y.-M., Xu, Z.-L., Hammock, B., 2020. Ecotoxicol. Environ. Saf. 188, 109904.
Gao, G., Chen, H., Zhu, L., Chai, Y., Ma, G., Wang, C., Hao, Z., Liu, X., Lu, C., 2017. Anal. Methods 9 (48), 6769–6776.
Gu, C., Wang, J., Guo, M., Sui, M., Lu, H., Liu, G., 2018. Water Res. 142, 354–362.
Guo, Z., Florea, A., Jiang, M., Mei, Y., Zhang, W., Zhang, A., Sandulescu, R., Jaffrezic-Renault, N., 2016. Coatings 6 (4).
Gutierrez-Serpa, A., Pacheco-Fernandez, I., Pasan, J., Pino, V., 2019. Separations 6 (4).
Hu, J., Tao, L., Deng, W., Liu, L., 2021. Flavour Fragrance J. 36 (1), 55–63.
Hu, Z., Jiang, X., Xu, F., Jia, J., Long, Z., Hou, X., 2016. Talanta 158, 276–282.
Iskierko, Z., Sharma, P.S., Prochowicz, D., Fronc, K., D'Souza, F., Toczydłowska, D., Stefaniak, F., Noworyta, K., 2016. ACS Appl. Mater. Interfaces 8 (31), 19860–19865.
Jia, J., Zhu, Q., Liu, N., Liao, C., Jiang, G., 2019. Chin. Sci. Bull. 64, 3467, 0023-074X.
Jin, H., Zhu, J., Chen, Z., Hong, Y., Cai, Z., 2018. Environ. Sci. Technol. 52 (2), 812–820.
Jurek, A., Leitner, E., 2018. Food Addit. Contam. 35 (11), 2256–2269.
Lai, D.Y., Kacew, S., Dekant, W., 2015. Food Chem. Toxicol. 80, 206–214.
Letcher, R.J., Chu, S., 2010. Environ. Sci. Technol. 44 (22), 8615–8621.
Li, A.J., Zhuang, T.F., Shi, W., Liang, Y., Liao, C.Y., Song, M.Y., Jiang, G.B., 2020. Sci. Total Environ. 707.
Li, M., Sun, P., Wu, Q., Liu, D., Zhou, L., 2018a. Environ. Sci.: Nano 5 (11), 2651–2662.
Li, S., Wang, X., He, Q., Chen, Q., Xu, Y., Yang, H., Lü, M., Wei, F., Liu, X., 2016a. Chin. J. Catal. 37 (3), 367–377.
Li, Y., Liu, J., Zhang, K., Lei, L., Lei, Z., 2018b. Ind. Eng. Chem. Res. 57 (2), 559–567.
Li, Y., Xu, J., Wang, L., Huang, Y., Guo, J., Cao, X., Shen, F., Luo, Y., Sun, C., 2016b. Sensor. Actuator. B Chem. 222, 815–822.
Liang, Q., Cui, S., Jin, J., Liu, C., Xu, S., Yao, C., Li, Z., 2018. Appl. Surf. Sci. 456, 899–907.
Liang, Q., Zhang, M., Zhang, Z., Liu, C., Xu, S., Li, Z., 2017. J. Alloys Compd. 690, 123–130.
Liu, A., Qu, G., Zhang, C., Gao, Y., Shi, J., Du, Y., Jiang, G., 2015. J. Chromatogr. A 1377, 92–99.
Liu, G., Chen, Z., Jiang, X., Feng, D.-Q., Zhao, J., Fan, D., Wang, W., 2016. Sensor. Actuator. B Chem. 228, 302–307.
Liu, H., Gao, W., Tian, Y., Liu, A., Wang, Z., Cai, Y., Zhao, Z., 2019. Talanta 191, 272–276.
Liu, H., Mu, L., Chen, X., Wang, J., Wang, S., Sun, B., 2017a. J. Agric. Food Chem. 65 (4), 986–992.
Liu, R., Lin, Y., Ruan, T., Jiang, G., 2017b. Environ. Pollut. 221, 227–233.
Lu, H., Xu, S., 2017. Biosens. Bioelectron. 92, 147–153.
Lu, J.F., He, M.J., Yang, Z.H., Wei, S.Q., 2018. Environ. Pollut. 242 (Pt A), 219–228.
Lu, W., Liu, J., Li, J., Wang, X., Lv, M., Cui, R., Chen, L., 2019. Analyst 144 (4), 1292–1302.
Mendes, T.P.P., Pereira, I., Ferreira, M.R., Chaves, A.R., Vaz, B.G., 2017. Anal. Methods 9 (43), 6117–6123.
Mettakoonpitak, J., Volckens, J., Henry, C.S., 2020. Anal. Chem. 92 (1), 1439–1446.
Noviana, E., Carrão, D.B., Pratiwi, R., Henry, C.S., 2020. Anal. Chim. Acta 1116, 70–90.
Noviana, E., Klunder, K.J., Channon, R.B., Henry, C.S., 2019. Anal. Chem. 91 (3), 2431–2438.
Noyes, P.D., Friedman, K.P., Browne, P., Haselman, J.T., Gilbert, M.E., Hornung, M.W., Barone Jr., S., Crofton, K.M., Laws, S.C., Stoker, T.E., 2019. Environ. Health Perspect. 127 (9), 095001.
Pungjunun, K., Chaiyo, S., Praphairaksit, N., Siangproh, W., Ortner, A., Kalcher, K., Chailapakul, O., Mehmeti, E., 2019. Biosens. Bioelectron. 143, 111606.
Qiao, P., Wang, X.-H., Gao, S., Yin, X., Wang, Y., Wang, P., 2020. Biosens. Bioelectron. 149, 111821.
Ramanayaka, S., Vithanage, M., Sarmah, A., An, T., Kim, K.-H., Ok, Y.S., 2019. RSC Adv. 9 (59), 34359–34376.
Ríos-Gómez, J., Ferrer-Monteagudo, B., López-Lorente, Á.I., Lucena, R., Luque, R., Cárdenas, S., 2018. J. Clean. Prod. 194, 167–173.
Sarker, M., Song, J.Y., Jhung, S.H., 2018. Chem. Eng. J. 331, 124–131.
Senthilkumaran, M., Eswaran, L., Saravanan, C., Puthiaraj, P., Rameshkumar, P., Muthu Mareeswaran, P., 2020. Mater. Chem. Phys. 239, 121995.
Shao, Y., Zhou, L., Wu, Q., Bao, C., Liu, M., 2017. J. Hazard Mater. 339, 418–426.
Shi, L., Rong, X., Wang, Y., Ding, S., Tang, W., 2018. Biosens. Bioelectron. 102, 41–48.
Song, D., Yang, R., Wang, H., Fang, S., Liu, Y., Long, F., Zhu, A., 2019. Biosens. Bioelectron. 126, 824–830.
Song, S., Song, M., Zeng, L., Wang, T., Liu, R., Ruan, T., Jiang, G., 2014a. Environ. Pollut. 186, 14–19.
Song, S.J., Song, M.Y., Zeng, L.Z., Wang, T., Liu, R.Z., Ruan, T., Jiang, G.B., 2014b. Environ. Pollut. 186, 14–19.
Tang, Y., Dong, L., Mao, S., Gu, H., Malkoske, T., Chen, B., 2018. ACS Appl. Energy Mater. 1 (6), 2698–2708.
Turiel, E., Martín-Esteban, A., 2019. TrAC Trends Anal. Chem. (Reference Ed.) 118, 574–586.
Wang, K., Liu, Z., Ji, P., Liu, J., Eremin, S.A., Li, Q.X., Li, J., Xu, T., 2016a. Anal. Methods 8 (39), 7265–7271.
Wang, L., Zhang, Z., Zhang, J., Zhang, L., 2016b. J. Chromatogr. A 1463, 1–10.
Wang, S., Niu, H., Cai, Y., Cao, D., 2018. Talanta 181, 340–345.
Wang, W., Abualnaja, K.O., Asimakopoulos, A.G., Covaci, A., Gevao, B., Johnson-Restrepo, B., Kumosani, T.A., Malarvannan, G., Minh, T.B., Moon, H.B., Nakata, H., Sinha, R.K., Kannan, K., 2015. Environ. Int. 83, 183–191.
Weatherston, J.D., Seguban, R.K.O., Hunt, D., Wu, H.-J., 2018. ACS Sens. 3 (4), 852–857.
Wu, Q., Li, M., Huang, Z., Shao, Y., Bai, L., Zhou, L., 2018. J. Ind. Eng. Chem. 60, 268–278.
Yakubu, S., Xiao, J., Gu, J., Cheng, J., Wang, J., Li, X., Zhang, Z., 2020. Sensor. Actuator. B Chem. 325, 128909.

Yang, Y., Lu, L., Zhang, J., Yang, Y., Wu, Y., Shao, B., 2014. J. Chromatogr. A 1328, 26–34.
Yang, Z., Tong, X., Feng, J., He, S., Fu, M., Niu, X., Zhang, T., Liang, H., Ding, A., Feng, X., 2019. Chemosphere 220, 98–106.
Ye, X., Wong, L.-Y., Kramer, J., Zhou, X., Jia, T., Calafat, A.M., 2015. Environ. Sci. Technol. 49 (19), 11834–11839.
Zhang, H., Luo, F., Wang, P., Guo, L., Qiu, B., Lin, Z., 2019a. Biosens. Bioelectron. 129, 36–41.
Zhang, K., Qing, J., Gao, H., Ji, J., Liu, B., 2017. Talanta 162, 52–56.
Zhang, Y., Chen, Z., Zhou, L., Wu, P., Zhao, Y., Lai, Y., Wang, F., Li, S., 2019b. J. Hazard Mater. 369, 770–779.
Zhao, Y., Pan, X., Zhang, L., Xu, Y., Li, C., Wang, J., Ou, J., Xiu, X., Man, B., Yang, C., 2017. RSC Adv. 7 (58), 36516–36524.
Zhu, Q., Jia, J., Wang, Y., Zhang, K., Zhang, H., Liao, C., Jiang, G., 2019a. Sci. Total Environ. 679, 61–69.
Zhu, Q., Wang, M., Jia, J., Hu, Y., Wang, X., Liao, C., Jiang, G., 2020. Environ. Sci. Technol. 54 (18), 11333–11343.
Zhu, Q.Q., Jia, J.B., Wang, Y., Zhang, K.G., Zhang, H., Liao, C.Y., Jiang, G.B., 2019b. Sci. Total Environ. 679, 61–69.